9th Asia-Pacific Conference on Wind Engineering
Auckland, New Zealand
3-7 December 2017

A Numerical Approach to The Simulation of Plate-type Wind-borne Debris

Feng Wang[1,2], Peng Huang[1], Mark Sterling[2] and Chris Baker[2]

[1] State Key Laboratory of Disaster Reduction in Civil Engineering
Tongji University, Shanghai 200092, China

[2]School of Engineering
University of Birmingham, Edgbaston, Birmingham B15 2TT, UK

Abstract

This paper presents a numerical analysis of the trajectories of plate-type wind-borne debris. Three-dimensional trajectories of the debris with an aspect ratio of two, released from a simple pitched-roof structure, are obtained by solving the Newton-Euler equations in conjunction with a simulated wind field. A series of simulations are undertaken for five different wind angles, i.e., 0°, 15°, 30°, 45° and 60°. In addition to the debris trajectories, the impact velocity at the time the debris strikes the ground is also calculated. It is noted that the actual trajectory of the debris and the impact velocity, appear to be a function of the angle of the approaching wind.

1 Introduction

The impact of wind-borne debris can be significant, as recently demonstrated by storm Doris in the UK [2]. Events such as this have led to the appreciation of the importance of this topic and have driven numerous experimental research in this area [13,19,21,16,20,1,10,11,4,5,17,18,22,8,9,14]. Initially, debris was generally considered as a one-dimensional particle [13,19] and subsequently extended to three-dimensions through the introduction of drag, lift and side forces [21,16,1,12]. Tachikawa [20] was fundamental in the development of this area and undertook a series of physical and numerical simulations. His research subsequently led to the identification of an important, dimensionless parameter governing the flight of the wind-borne debris [4], i.e., the Tachikawa number. In 2002, Wills et al. [24] identified three general categories (compact, sheet (plate) and rod) which, in general, can be used to describe the behaviour of wind-borne debris.

Numerical simulations have tended to follow the experimental research and have provided a greater insight into the complexities of wind-borne debris flight. For example, see Kakimpa et al. [7], Moghim and Caracoglia [14] and Huang et al. [6]. Whilst insightful, these simulations can be resource intensive and it is suggested that a simpler approach would be of benefit to the engineer, hence the research outlined below.

In summary, significant progress has been made in the study of wind-borne debris over the past 40 years. In the current research, a new approach has been developed and is applied to plate debris with an aspect ratio of 2. The numerical model is outlined in Section 2 with initial results shown in Section 3. Finally, some general conclusions are presented in Section 4.

2 Flight Equations and Initial Conditions

2.1 Flight Equations and Coordinate Systems

The current research applies the classical Newton-Euler equations to a rigid body subjected to a simulated wind field:

$$m\frac{d\mathbf{V}}{dt} = \mathbf{F}_g \tag{1}$$

$$\mathbf{I}_p \frac{d\boldsymbol{\omega}_p}{dt} = \mathbf{M}_P - \boldsymbol{\omega}_p \times \mathbf{I}_p\boldsymbol{\omega}_p \tag{2}$$

where m represents the mass of the body, t is the time, $\mathbf{V}$ is the velocity vector, $\mathbf{F}$ is the force vector, $\mathbf{I}$ is the angular momentum vector, $\mathbf{M}$ is the moment vector and $\boldsymbol{\omega}$ is the angular velocity vector. The subscripts g and p are used to denote a vector expressed in a global inertial reference frame (X_g, Y_g, Z_g) and body-fixed coordinate (X_p, Y_p, Z_p), respectively. Finally, X, Y and Z represent the longitudinal, vertical and lateral direction respectively.

The position of the debris in a fixed-body coordinate system is transferred to a global inertial reference frame, using the rotational quaternions method in order to avoid any potential singularities of parameters with respect to Euler angles [6]. The normal force coefficients which determine the force on the plate debris are derived from the study of Richards et al. [18].

In order to solve equations (1) and (2) in conjunction with a simulated wind field (section 2) the Runge-Kutta method is employed with a time step of 0.004 s.

2.2 Initial Conditions

In what follows, a mean wind speed of 4.5 m/s has been adopted. The wind field is simulated based on an approach initially outlined by Deodatis [3]. In what follows, $\boldsymbol{W}$ denotes the wind velocity with W_x, W_y and W_z corresponding to the longitudinal, vertical and lateral components respectively.

Figure 1 shows an example of the simulated longitudinal, vertical and lateral wind velocity time histories based on the method of Deodatis [3], whilst figure 2 shows the corresponding spectra. The turbulence intensity of the three simulated velocity components are 12%, 6% and 12%, and the corresponding turbulence integral scales are 0.45, 0.54 and 0.4 m for the longitudinal, vertical and lateral components respectively. As indicated in figure 2, the simulated spectra correspond well with the Von Karman [23] spectra.

In figure 3, the definition of the wind direction and initial (starting) position of the debris is shown. The low-rise building model has dimensions (length, height and width) of 0.2×0.213×0.2 m and the plate-type debris has a dimension of 0.02×0.0008×0.04 m. (These dimensions have been chosen, since the building represents a 1:30 scale model which will subsequently be used in a series of wind tunnel experiments (not reported herein)). The building model has a roof pitch of 1:3 and the height to the eaves is 0.18 m. The debris is made from balsa wood with a weight of 0.2 g and a density of 312.5 kg/m^3.

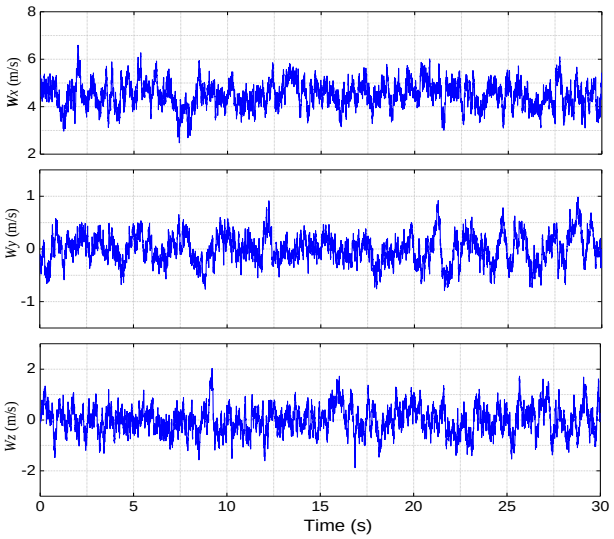

Figure 1. A sample of the simulated longitudinal, vertical and lateral wind velocity time histories.

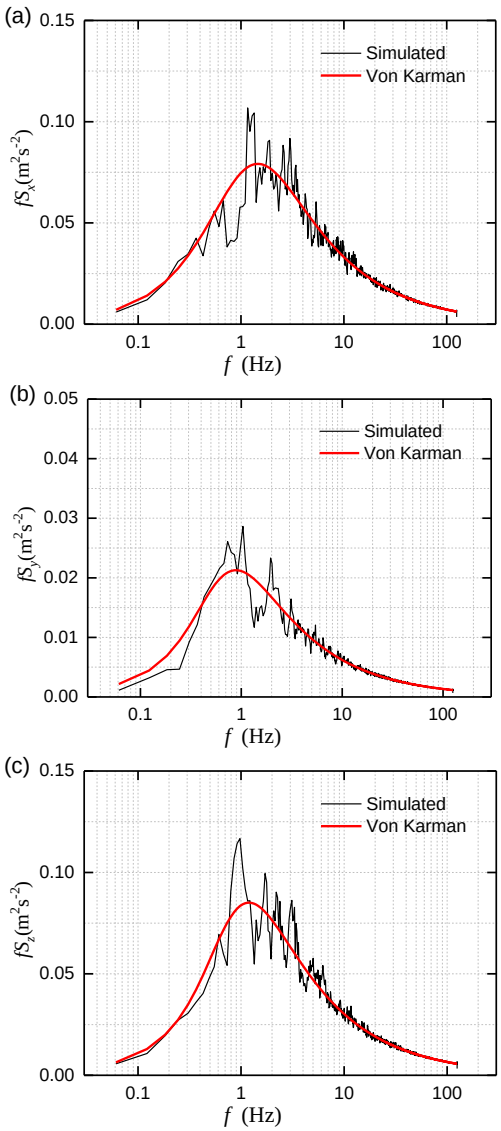

Figure 2. An example of the simulated of (a) longitudinal, (b) vertical and (c) lateral wind spectrum.

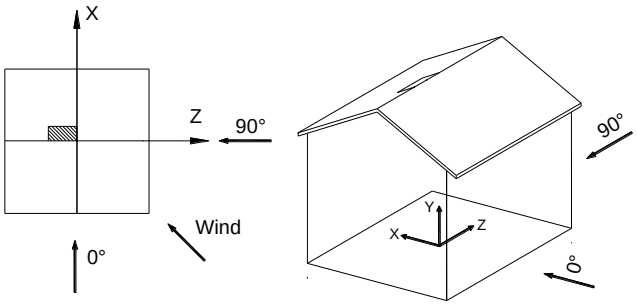

Figure 3. An illustration showing the model building, definition of the wind directions and initial position of the debris.

3 Results of debris trajectories

The probabilistic flight trajectories of the debris are simulated using the method briefly outlined in the previous section. For each wind direction, 100 possible trajectories are calculated in order to analyse the flight characteristics. Figure 4 shows the flight path of thirty simulations. In figure 4, the centre of the debris is shown for the sake of simplicity. In figure 4 the colour represents the debris velocity. It is evident from figure 4 that the velocity of the debris is relatively low at the early stage of the flight and subsequently increases to approximately the wind speed. Figures 4a to 4c illustrate that there is relatively little spread in the trajectory paths for 0°, 15° and 30°, however, as the angle of attack increases the variation in trajectories also increases. In addition, it can be observed that for higher angles of attack, the debris "climbs" into the air before it starts its downwards journey—this has implications for the final impact velocity as can be observed in figure 5 and table 1.

Figure 5 shows the longitudinal, vertical and lateral impact debris velocities for 100 simulation results with respect to the 5 different wind directions considered. In figure 5a (and table 1), it is evident that, in general, the mean dimensionless debris speed is greatest for 0° and decreases as the angle of attack increases, although there is, little discernible difference in magnitude of the mean dimensionless debris speed between 30° and 45°. Figures 5b–5d shows the contributions of the various velocity components to the debris speed. In addition, table 1 shows the mean, maximum and corresponding standard deviation for the data in figure 5.

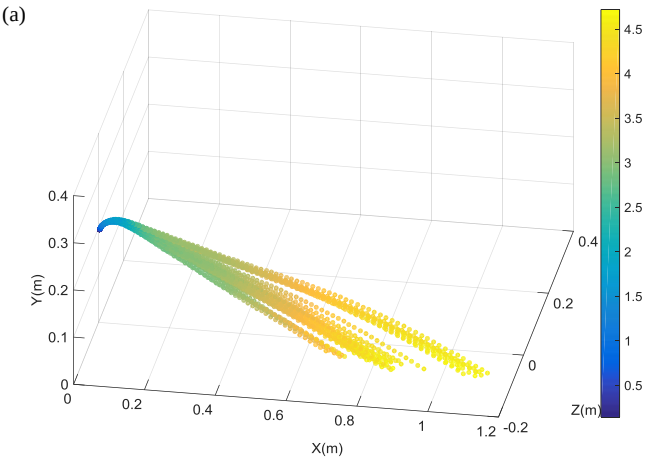

Figure 4. Thirty examples of positions of debris center and flight velocity of debris (a) 0°, (cont. over)

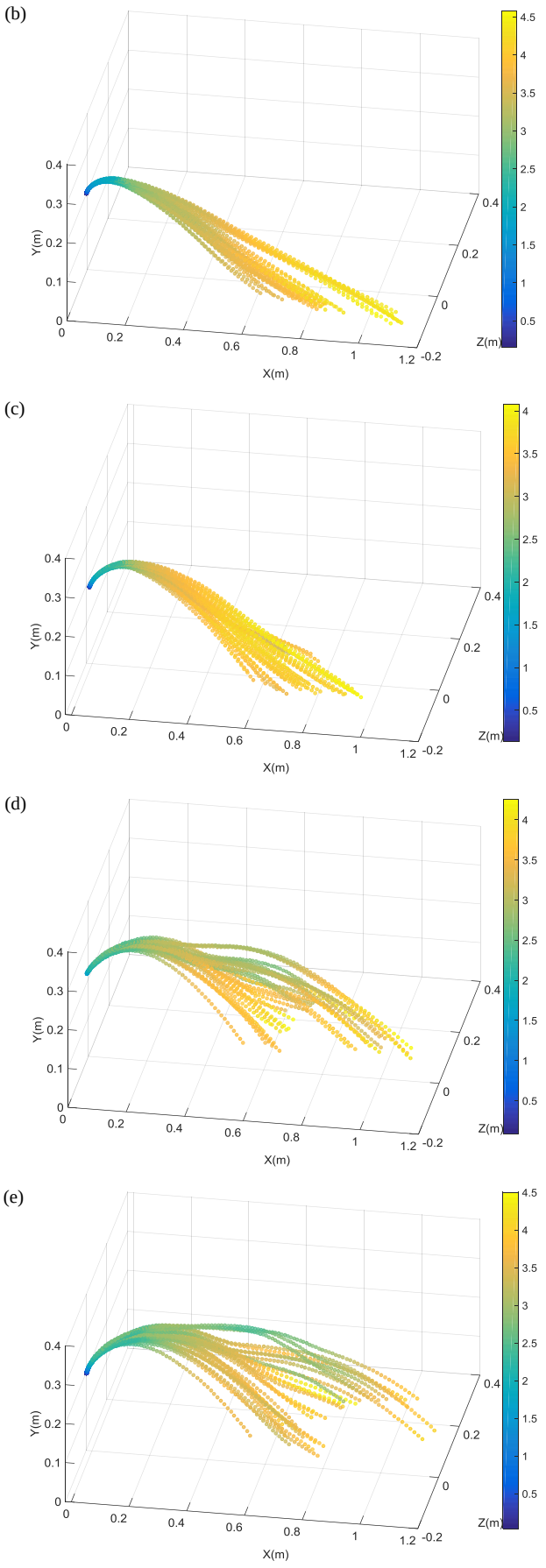

Figure 4 (cont.). Thirty examples of positions of debris center and flight velocity of debris (b) 15°, (c) 30°, (d) 45°, (e) 60°.

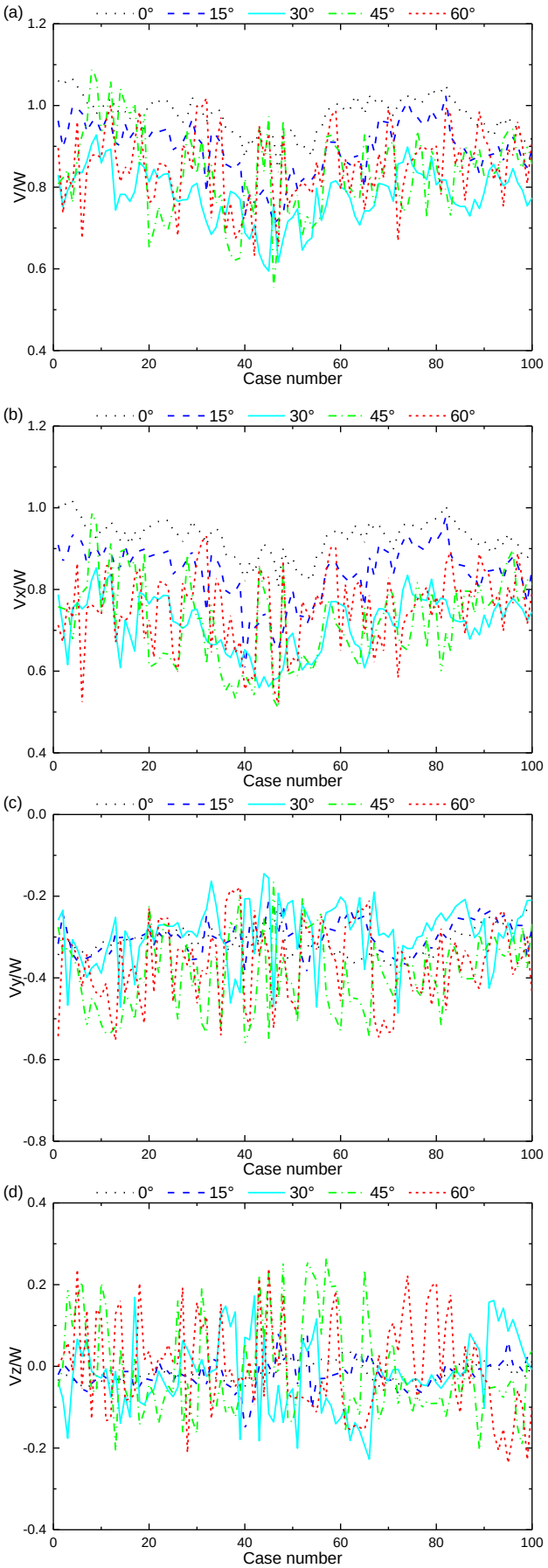

Figure 5. Dimensionless (a) resultant, (b) longitudinal, (c) vertical and (d) lateral impact velocity at landing positions of 100 simulations under 5 wind directions.

Impact velocity		Wind direction				
		0°	**15°**	**30°**	**45°**	**60°**
Mean	V/W	0.98	0.90	0.78	0.83	0.85
	Vx/W	0.93	0.84	0.71	0.72	0.75
	Vy/W	-0.31	-0.30	-0.29	-0.39	-0.36
	Vz/W	-0.02	-0.02	-0.02	-0.01	0.00
Max	V/W	1.07	1.02	0.93	1.09	1.02
	Vx/W	1.02	0.98	0.85	0.99	0.93
	Vy/W	-0.38	-0.39	-0.49	-0.57	-0.55
	Vz/W	0.04	0.08	0.17	0.26	0.24
Std	V/W	0.04	0.07	0.07	0.11	0.09
	Vx/W	0.04	0.07	0.07	0.10	0.09
	Vy/W	0.03	0.04	0.07	0.09	0.10
	Vz/W	0.02	0.04	0.09	0.12	0.12

Table 1. Dimensionless debris impact speed and corresponding velocity components.

4 Conclusions

This paper analysed the three-dimensional positions of plate-like debris subjected to a simulated wind field. For wind directions of 0° and 15°, the debris flight trajectories are all predicted to be reasonably flat and quick, whereas the trajectories for 30°, 45°, and 60° cases appear to be more complex. The mean dimensionless longitudinal impact velocity has its maximum and minimum value of 0.93 and 0.71 under wind directions of 0° and 30°, respectively. The maximum mean dimensionless vertical impact velocity is -0.57 at 60°. The maximum dimensionless total and lateral impact velocity can reach 1.09 and 0.26 at 45°.

The paper sets forth a simple and possibly highly effective approach, which could subsequently be used in a design framework to invest wind-borne debris loading.

Acknowledgments

This project is supported by the Chinese National Natural Science Foundation (Nos. 51378396 and 51678452), and the study of the first author in University of Birmingham was fund by China Scholarship Council, which are gratefully acknowledged.

References

[1] Baker, C.J., The debris flight equations, *J. Wind Eng. Ind. Aerodyn.*, **95**, 2007, 329-353.

[2] BBC (2017), http://www.bbc.co.uk/news/uk-england-39079127, Last accessed 26th April 2017.

[3] Deodatis, G., Simulation of ergodic multivariate stochastic processes, *J. Eng. Mech.*, **122**, 1996, 778 – 787.

[4] Holmes, J.D., Baker, C.J. and Tamura, Y., Tachikawa number: A proposal, *J. Wind Eng. Ind. Aerodyn.*, **94**, 2006a, 41-47.

[5] Holmes, J.D., Letchford, C.W. and Lin, N., Investigations of plate-type windborne debris—Part II: Computed trajectories, *J. Wind Eng. Ind. Aerodyn.*, **94**, 2006b, 21-39.

[6] Huang, P., Wang, F., Fu, A. and Gu, M., Numerical simulation of 3-D probabilistic trajectory of plate-type wind-borne debris, *Wind Struct.*, **22**, 2016, 17-41.

[7] Kakimpa, B., Hargreaves, D.M., Owen, J.S., An investigation of plate-type windborne debris flight using coupled CFD–RBD models, Part II: Free and constrained flight, *J. Wind Eng. Ind. Aerodyn.*, **111**, 2012, 104-116.

[8] Kordi, B. and Kopp, G.A., Effects of initial conditions on the flight of windborne plate debris, *J. Wind Eng. Ind. Aerodyn.*, **99**, 2011, 601-614.

[9] Kordi, B., Traczuk, G. and Kopp, G.A., Effects of wind direction on the flight trajectories of roof sheathing panels under high winds, *Wind and Struct.*, **13**, 2010, 145-167.

[10] Lin, N., Holmes, J.D. and Letchford, C.W., Trajectories of wind-borne debris in horizontal winds and applications to impact testing, *J. Struct. Eng.*, **133**, 2007, 274-282.

[11] Lin, N., Letchford, C. and Holmes, J., Investigation of plate-type windborne debris. Part I. Experiments in wind tunnel and full scale, *J. Wind Eng. Ind. Aerodyn.*, **94**, 2006, 51-76.

[12] Martinez-Vazquez, P., Baker, C. J., Sterling, M., Quinn, A. D and Richards, P. J., Aerodynamic Forces on Fixed and Rotating Plates, *J. Wind Struct*., **13**, 2010, 127-144.

[13] McDonald, J.R., Mehta, K.C. and Minor, J.E., *Tornado-resistant design of nuclear power-plant structures*, Texas Tech. Univ., Austin, 1974.

[14] Moghim, F. and Caracoglia, L., Effect of computer-generated turbulent wind field on trajectory of compact debris: A probabilistic analysis approach, *Eng. Struct.*, **59**, 2014, 195-209.

[15] Moghim, F., Xia, F.T. and Caracoglia, L., Experimental analysis of a stochastic model for estimating wind-borne compact debris trajectory in turbulent winds, *J. Fluid Struct.*, **54**, 2015, 900-924.

[16] Redmann, G.H., Radbill, J.R., Marte, J.E., Dergarabedian, P. and Fendell, F.E., *Wind field and trajectory models for tornado-propelled objects*, Electrical Power Research Institute, Technical Report 1, Palo Alto, CA, 1978.

[17] Richards, P., *Steady aerodynamics of rod and plate type debris*. Proceedings of the Seventeenth Australasian Fluid Mechanics Conference, Auckland, New Zealand, 2010, 5-9.

[18] Richards, P.J., Williams, N., Laing, B., McCarty, M. and Pond, M., Numerical calculation of the three-dimensional motion of wind-borne debris, *J. Wind Eng. Ind. Aerodyn.*, **96**, 2008, 2188-2202.

[19] Simiu, E. & Cordes, M, *Tornado-Borne Missile Speeds*. National Bureau of Standards, 1976.

[20] Tachikawa, M., A method for estimating the distribution range of trajectories of wind-borne missiles, *J. Wind Eng. Ind. Aerodyn.*, **29**, 1988, 175-184.

[21] Twisdale, L.A., Dunn, W.L., Davis, T.L., Tornado missile transport analysis, *Nucl. Eng. Des.*, **51**, 1979, 295-308.

[22] Visscher, B.T. and Kopp, G.A., Trajectories of roof sheathing panels under high winds, *J. Wind Eng. Ind. Aerodyn.*, **95**, 2007, 697-713.

[23] Von Karman T, *Progress in the statistical theory of turbulence*, Proceedings of the National Academy of Sciences, **1948**, 34, 530-9.

[24] Wills, J.A.B., Lee, B.E. and Wyatt, T.A., A model of wind-borne debris damage, *J. Wind Eng. Ind. Aerodyn.*, **90**, 2002, 555-565.